PROCEEDINGS OF SPIE REPRINT

SPIE—The International Society for Optical Engineering

Reprinted from

Optical Remote Sensing of the Atmosphere and Clouds II

9–12 October 2000
Sendai, Japan

Volume 4150

Temperature and pressure retrievals from O_2 *A*-band absorption measurements made by ILAS: Retrieval algorithm and error analyses

Takafumi Sugita,[§a] Tatsuya Yokota,[a] Teruyuki Nakajima,[b] Hideaki Nakajima,[a] Katsunori Waragai,[c] Makoto Suzuki,[d] Akiyoshi Matsuzaki,[e] Yasuhiro Itou,[f] Hisaya Saeki,[f] and Yasuhiro Sasano[a]

a) National Institute for Environmental Studies, Tsukuba, Japan
b) Center for Climate System Research, University of Tokyo, Tokyo, Japan
c) Matsushita Electric Industrial Co., Ltd., Kawasaki, Japan
d) Earth Observation Research Center, National Space Development Agency of Japan, Tokyo, Japan
e) Faculty of Engineering, Mie University, Tsu, Japan
f) Fujitsu FIP Corporation, Tokyo, Japan

ABSTRACT

A visible grating spectrometer of the Improved Limb Atmospheric Spectrometer (ILAS) aboard the Advanced Earth Observing Satellite (ADEOS) measured atmospheric absorption spectra at a wavelength region from 753 nm to 784 nm, including the molecular oxygen (O_2) *A*-band centered at 762 nm, with a spectral resolution of 0.17 nm. Temperature and pressure profiles throughout the stratosphere were retrieved from the satellite solar occultation measurements of the O_2 *A*-band absorption spectra. Based on simulation studies, root-sum-square errors associated with several systematic uncertainties in spectroscopic databases and instrument functions were estimated to be 4 K for temperature and 4% for pressure in the stratosphere. Current problems in this retrieval are also presented through comparisons with correlative temperature measurements.

Keywords: remote sensing, retrieval, temperature, molecular oxygen *A*-band, ILAS, solar occultation

1. INTRODUCTION

The Improved Limb Atmospheric Spectrometer (ILAS), which was developed by Environment Agency of Japan, is one of the atmospheric remote sensing instruments on board the Japanese Advanced Earth Observing Satellite (ADEOS). ADEOS was launched from Tanegashima island, Japan (30°N, 131°E) in August, 1996, and put into a sun-synchronous polar orbit. Since ILAS makes use of the solar occultation technique, it is suitable for measuring high latitudes in both hemispheres (57-73°N and 64-88°S). The operational measurements started at the end of October, 1996. By June 1997, when the ADEOS stopped its operation due to solar paddle failure, more than 5800 occultation events had successfully been made.[1] ILAS consists of two grating spectrometers (covering 6.21-11.77 μm by an infrared one and 753-784 nm by a visible one, respectively) and a sun edge sensor (SES).[1,2]

The infrared grating spectrometer of ILAS measured atmospheric absorption spectra of ozone (O_3), nitric acid (HNO_3), nitrous oxide (N_2O), nitrogen dioxide (NO_2), methane (CH_4), water vapor (H_2O), and so on. In order to retrieve the volume mixing ratio profiles of these species, temperature should be known accurately. For this purpose, the visible spectrometer measured atmospheric absorption spectra of the oxygen (O_2) *A*-band centered at 762 nm. An advantage of the use of O_2 instead of carbon dioxide (CO_2) for temperature sensing is that O_2 has a very stable composition and a more uniform distribution (both horizontally and vertically) from the stratosphere to the mesosphere (up to about 80 km altitude). Recent spectroscopic data for the O_2 *A*-band[3-5] have revealed good accuracy comparable to those for CO_2 bands used for temperature sensing (e.g., 16 μm or 4.3 μm band). Originally, Wallace and Hunten[6] and Heller et al.[7] inferred temperatures in the mesosphere from the O_2 *A*-band dayglow measurements made by rockets. Matsuzaki et al.[8] derived temperature at 21 km altitude from the O_2 *A*-band absorption spectrum measured by a rocket-borne radiometer. Recently, Pitts and Thomason[9] and Pitts[10] have suggested that theoretical simulations for multi-spectral measurements of the O_2 *A*-band in the Stratospheric Aerosol and Gas Experiment (SAGE) III will meet scientific requirements for temperature and pressure measurements. Theoretical simulations for the O_2 *A*-band measurements of ILAS have already shown to have errors within *2 K at altitudes* up to 40 km.[11]

§ Send correspondence to T.S.: e-mail: tsugita@nies.go.jp

Optical Remote Sensing of the Atmosphere and Clouds II, Yasuhiro Sasano, Jinxue Wang, Tadahiro Hayasaka, Editors, Proceedings of SPIE Vol. 4150 (2001) © 2001 SPIE · 0277-786X/01/$15.00

This paper describes the current status of the retrieval scheme, error analyses, and preliminary comparisons with some correlative temperature measurements, as well as some results of the performance of the visible spectrometer in orbit.

2. INSTRUMENTATION AND DATA PROCESSING

2.1. Visible spectrometer

Specifications of the visible spectrometer of ILAS are listed in Table 1. A schematic optical system of the spectrometer is illustrated in Figure 1. The spectrometer consists of a holographic concave grating (F/8.0, f = 400 nm, 1803 grooves/mm) with a 1024-pixel MOS photo diode array detector, which covers wavelength regions between 753 and 784 nm with a 0.15 nm FWHM resolution. However, for instrumental temperatures (~ 288 K) in orbit, the FWHM was broadened by about 15%, resulting in a 0.17 nm resolution. The visible sun light is reflected (F/4.0) in front of the beam splitter and focused (F/8.0) on the entrance slit of the spectrometer using four lens transfer optics. The spectrometer uses a part of the 12 cm telescope (3 cm in effective diameter) to reduce the sun light and to obtain better imaging quality.

2.2. Calibration of wavelength center of instrument functions

We have found that the wavelength center of the visible spectrometer changed with increasing instrument temperature of about 5 K in orbit, after the initial check-out of ILAS instruments. This is explained by the high dispersion of the spectrometer and its optical layout. The diffracted light is tilted against a projection plane of the detector as shown in Figure 1. Therefore, heat expansion of the optical base makes the diffracted wavelength change, through changes in L and Y0.

The change in instrument temperatures near the optical base was also about 5 K from November 1996 through June 1997. Therefore, we need to calibrate the wavelength center of the instrument functions as a function of time. We have calibrated the diffracted wavelength at each pixel number by the aid of solar spectra observed by ILAS in the exoatmosphere, as briefly described below. Wavenumbers of the solar lines were identified in high resolution FTIR solar spectra observed at Kitt Peak.[12] These Kitt Peak solar line data were convoluted by the instrument functions of the visible spectrometer. The convoluted solar spectra were then compared with the solar spectra in the ILAS exoatmospheric data. Minimizing residuals between the central position of the two solar spectra (i.e., the ILAS and the Kitt Peak data) at 13 selected wavenumber regions (which include strong and distinct solar lines) outside of the O_2 *A*-band, the diffracted wavelength (i.e., principal ray) at each pixel number is determined (i.e., calibrated). The error in the wavelength center is estimated to be +/- 0.012 nm (0.4 pixel). A detailed description of the procedure is given in Nakajima et al.[13] We performed this calibration for one occultation event per week both for sunrise and sunset modes separately. In total, 72 instrument functions (36 weeks x 2 occultation modes) were assigned for each 1024 pixels, and used for events that occurred within the respective weeks.

2.3. Measured signals

The Level 0 data, which was acquired at 12 Hz, is first filtered by some criteria in terms of anomalous and/or missing values. These filtered data are called Level 0A data. The Level 1 data, a pseudo-transmittance, are calculated from the Level 0A data for each detector element by the following equation:

$$\tau_o(t) = \{I_a(t) - I_z(t)\} / \{I_o(t) - I_z(t)\} \tag{1}$$

where

$$I_z(t) = a_z \times t + b_z,\ I_o(t) = a_o \times t + b_o$$

$I_a(t)$ is the measured atmospheric spectrum at each 12-Hz measurement time, t. $I_o(t)$ and $I_z(t)$ are the measured solar spectrum out of the atmosphere (taken around tangent heights of 120 km) and the measured spectrum for zero incoming radiance from deep space at t, respectively. For each satellite sunrise event, the I_z is measured first and then the I_a is measured followed by the I_o measurement. To conclude, the I_z is measured again. A reverse measurement sequence is performed at each satellite sunset event. It is obvious that the I_z and I_o signals had drifted slightly during the each occultation event due to changes in the instrument temperatures. Therefore, we have to know accurate signals of the I_z and I_o at the time of the I_a measurements. We have corrected the I_z and I_o signals, respectively, by interpolating and extrapolating those signals to every I_a measurement time. As the result, $\tau_o(t)$ can be calculated at each I_a measurement.

Figure 2 shows typical signals for $I_a(t)$ at measurement times that correspond to tangent heights of 10, 15, 20, 30 and 70 km altitudes observed at a sunset occultation event on November 30, 1997. The spectrum consists of an absorption spectrum caused by O_2 molecules in the center and a continuously-varying baseline component, to which aerosol extinction (Mie scattering), scattering due to air molecules (Rayleigh scattering), and absorption due to ozone in the Wulf-band[14] contribute. The absorption feature of the O_2 *A*-band is strong even at the 70 km tangent height. This confirms the selection of this band as a temperature and pressure sensor. From this figure, we can also see some solar lines.

Figure 3 shows a typical signal-to-noise ratio (SNR) of the spectrometer, defined by an average signal divided by 1 sigma standard deviation of the I_o signals of 180 major frames (the duration is about 15 seconds) observed at a sunset occultation event on February 19, 1997.

2.4. Retrieval strategies

An algorithm flow for retrieving temperature and pressure profiles from the ILAS visible spectrometer data is shown in Figure 4. Since ILAS made atmospheric measurements with the solar occultation technique, it is assumed in the data processing that the atmosphere is horizontally homogeneous and has variations only in the vertical direction. The atmosphere is divided into atmospheric layers with 1 km thickness between the lowest measurable altitudes (depending on the occultation events, usually 12 km in the satellite sunrise mode and 9 km in the satellite sunset mode) and 71 km. τ_o, which is derived by Equation (1), is first corrected with a baseline subtraction method, which is described in the Appendix of Hayashida et al.,[15] resulting in "baseline-corrected transmittance", defined as τ'_o. In this procedure, data from Brion et al[16] is used for an absorption cross-section spectrum due to ozone in the Wulf band.

Temperature and pressure profiles are retrieved to minimize the residual between observed transmittance and simulated one at each atmospheric layer by applying the onion peeling method for vertical inversion.

$$\sum w\{\tau'_o - \tau'_c\}^2 \rightarrow \min \tag{2}$$

where

$$\tau'_c = \frac{\int_{\Delta\nu} I_s(\nu) * \tau_c(\nu) * F(\nu) d\nu}{\int_{\Delta\nu} I_s(\nu) * F(\nu) d\nu}$$

Here, I_s is the source function of the solar ray, τ'_c is the calculated atmospheric transmittance, and F is the instrument function of the detector. w is a weight coefficient for each pixel (here, w is set to 1). A detailed description of a calculation for τ'_c is given in the Appendix. For the database of I_s, we used data in the Version 3.5 MODTRAN.[17] It also includes the solar lines with 1 cm^{-1}. τ'_c and I_s are both then shifted by about 0.015 nm due to the Doppler effect (described below). Then, τ'_c is convoluted by I_s. Finally, a simulated atmospheric transmittance convolved by F is divided by a simulated exoatmospheric spectrum convolved by F, and it is defined here as τ'_c.

Tangent height assignment. For the first stage of this retrieval algorithm, we need to know tangent height for each major frame as a time series in 12 Hz. As shown in Figure 4, the tangent height is determined from a combined method of two assignments. The tangent height is assigned by the sun-edge sensor (SES) data in the Version 4.20 algorithm,[15] whereas it is determined by the visible spectrometer data and meteorological data in the Version 3.10 algorithm.[2] Here, the tangent height determined by the former method is defined as TH(SES), and the latter is defined as TH(VS).

The TH(SES) is determined by the following way. The SES supplies information on angle difference between the top edge of the sun and the IFOV direction from its 1024 detector array data. This angle data, together with astronomical data on the sun and earth positions, and the satellite position data, is used to geometrically calculate tangent heights, when atmospheric refraction effects are correctly taken into consideration. The refraction calculation is made at 1 km intervals along the limb-path with the ray trace technique, and also at each atmospheric layer boundary along the path by using Snell's law. In this ray trace calculation, the shape of the earth is assumed to be a sphere with the local radius at the latitude of the measurement point. For this refraction calculation, we used temperature and pressure profiles from the United Kingdom Met. Office (UKMO) stratospheric assimilation data.[18] Above about 55 km, the 1986 CIRA (COSPAR International Reference Atmosphere) data[19] are used as these profiles.

A determination of the TH(VS) is based on an integrated transmittance comparison, in which an integral of τ'_o over the P-branch region of the O_2 A-band is compared with that of τ'_c as a function of geometric altitude using the independent meteorological data (i.e., the UKMO data). The ray-path calculated by the above method is also used for the calculation of τ'_c. The 1996 HITRAN compilation (hereafter referred to as HT96) is used for the O_2 A-band spectroscopic line parameters.[20]

When measuring a solar spectrum through the atmosphere or space by ILAS, the measured spectrum is shifted due to the Doppler effect. The average flight speed of ADEOS is 7.4 km/sec and the speed vector towards the sun is about 6.0 km/sec. Thus the frequency difference between satellite sunrise and sunset occultation events becomes 0.5 cm^{-1} at 13157.63 cm^{-1} (760 nm). This is comparable with the dispersion (0.03 nm/pixel) of the spectrometer. The calculated transmittance is then shifted by those amounts at each major frame.

Comparisons of the TH(SES) with the TH(VS) at a certain major frame showed that their differences varied by season. These facts may be explained by changes in the IFOV position relative to the SES detector array, which depend on the instrument temperature.[21] To solve this problem, we introduced a correction method to the Version 4.20, where the IFOV position on the SES was determined at every occultation event by assuming the TH(VS) was correct at a certain reference altitude. We set 30 km altitude as the reference, where errors in the UKMO temperature are very small (within +/- 1K)[18] and the integral of transmittance theoretically calculated is less sensitive to changes in temperature.[21] A detailed description for determining the tangent height will be given by Nakajima et al.[21] The tangent height is then assigned for each major frame.

Spectral fitting. To minimize the residual between τ'_o and τ'_c in Equation (2), we used the Gauss-Newton non-linear least squares method for the spectral fitting. Since we used the onion-peeling method for the vertical profiling, we consider temperature and pressure at the layer of tangent height for each 1 km layer. Therefore, τ'_o and τ'_c can be expressed as $\tau'_o(p_o, T_o)$ and $\tau'_c(p_c, T_c)$, respectively. Here, p_o (p_c) and T_o (T_c) are observed (calculated) pressure and temperature at the layer of tangent height, respectively. τ'_c can be expanded by the Taylor series of order 1 as Equation (3).

$$\tau'_o(p_o,T_o) = \tau'_c(p_c,T_c) + \left(\frac{\partial \tau'_c}{\partial p_c}\Delta p_c + \frac{\partial \tau'_c}{\partial T_c}\Delta T_c \right) \tag{3}$$

$$\Delta\tau = \tau'_o - \tau'_c = \frac{\partial \tau'_c}{\partial p_c}\Delta p_c + \frac{\partial \tau'_c}{\partial T_c}\Delta T_c \tag{4}$$

where

$$\frac{\partial \tau'_c}{\partial p_c} \cong \frac{\tau'_c(p_c+\delta p_c,T_c)-\tau'_c(p_c,T_c)}{\delta p_c}, \quad \frac{\partial \tau'_c}{\partial T_c} \cong \frac{\tau'_c(p_c,T_c+\delta T_c)-\tau'_c(p_c,T_c)}{\delta T_c} \tag{5}$$

Equation (5) can be calculated numerically. Since Equation (4) is true for each 1024 pixels, Δp_c and ΔT_c can be calculated as follows, .

$$\mathbf{x} = \left(\mathbf{J}^{\mathrm{T}}\mathbf{W}\mathbf{J}\right)^{-1}\mathbf{J}^{\mathrm{T}}\mathbf{W}\mathbf{y} \tag{6}$$

where

$$\mathbf{y} = \begin{pmatrix} \Delta\tau'_1 \\ \Delta\tau'_2 \\ \vdots \\ \vdots \\ \Delta\tau'_{1024} \end{pmatrix}, \quad \mathbf{J} = \begin{pmatrix} \frac{\partial\tau'_1}{\partial p_c} & \frac{\partial\tau'_1}{\partial T_c} \\ \frac{\partial\tau'_2}{\partial p_c} & \frac{\partial\tau'_2}{\partial T_c} \\ \vdots & \vdots \\ \vdots & \vdots \\ \frac{\partial\tau'_{1024}}{\partial p_c} & \frac{\partial\tau'_{1024}}{\partial T_c} \end{pmatrix}, \quad \mathbf{x} = \begin{pmatrix} \Delta p_c \\ \Delta T_c \end{pmatrix}$$

Here, **y** is the difference between observed and simulated transmittances for each pixel, **J** is the Jacobian, **x** is the difference between initial and deduced values, and **W** is a weight coefficient matrix. Here, **W** is set to **I**, a unit matrix. To calculate **J**,

we used 10% of the values of T_c and p_c as values of δT_c and δp_c. For initial temperature and pressure, we used the co-located UKMO data.

For convergence criteria, when both of the parameters in Equation (7) are met for some values of ε_p and ε_T, the repetition is stopped and temperature and pressure at that layer are determined. For values of ε_p and ε_T, we used 0.01 and 0.1 K, respectively. If this convergence criterion is not met for 15 repetitions, unconverged values for pressure and temperature were used to solve the lower layers. Since we use the onion-peeling method for vertical inversion, this procedure is repeated for lower layers.

$$\Delta p_c / p_c < \varepsilon_p,\ \Delta T_c < \varepsilon_T \tag{7}$$

Error analysis. Error is calculated from the final residuals of convergence in the non-linear least squares method as in Equation (8).

$$\sigma = diag(\mathbf{\Omega})^{1/2} \tag{8}$$

where $\mathbf{\Omega}$ is the covariance matrix.

$$\mathbf{\Omega} = \mathbf{\Phi}(\mathbf{J}^{\mathrm{T}}\mathbf{W}\mathbf{J})^{-1}$$

where $\mathbf{\Phi}$ is the weighted sum of squares of fitting residuals.

$$\mathbf{\Phi} = \frac{\mathbf{y}^{\mathrm{T}}\mathbf{W}\mathbf{y}}{n-p}$$

where n is the number of pixels (n = 1024) and p the number of parameter (p = 2). The errors associated with this fitting residuals between the simulated and observed transmittances (i.e., the internal error) in the P-branch pixel region were 2 K and 4 K for temperature and 1% and 3% for pressure at altitudes of 20 km and 40 km, respectively.

3. RETRIEVAL RESULTS AND DISCUSSION

Temperatures retrieved by ILAS were compared with those retrieved by the Halogen Occultation Experiment (HALOE). HALOE uses the 2.8 μm CO_2 band to retrieve temperature, and the uncertainty of typical measurements is estimated to be 5 K for altitudes from 35 to 80 km.[25] Although their satellite orbits are different, relatively tight coincidences between the two measurements occurred in November/December, 1996 and January/February, 1997 in the southern hemisphere and in March, May, and June, 1997 in the northern hemisphere. We used the 3 tightest coincidence pairs from each month for this comparative study. The time and space differences ranged from 0.0 to 7.0 hours and from 30 to 250 km, respectively. Preliminary comparisons of the Version 5.10 ILAS temperatures with the Version 19 HALOE temperatures in the middle stratosphere show relatively good agreement between the two in the southern hemisphere, although with occasional differences reaching +/- 10 K. However, in the northern hemisphere, statistically significant differences between the two were evident, reaching a 20 K cooling bias at 50 km in the ILAS data. Figure 5 shows temperature profiles measured by ILAS and HALOE in March, 1997 in the northern hemisphere as a representative. The error bars in the ILAS profiles show the error values defined in section 2.4. According to potential vorticity (PV) maps from the UKMO data, the both measurements at a 475 K potential temperature level were made outside, at inner boundary, and outer boundary of the polar vortex on March 27, 28, and 29, 1997, respectively.

We examined the following four items as possible factors to take place such a systematic difference. As can be seen from Figure 4, several databases are used for the temperature and pressure retrievals: namely, the O_2 *A*-band line parameters, the O_3 absorption cross-sections, and the solar spectrum. Uncertainties in these databases directly influence to error in the data product as a systematic way. We examined the impact of the uncertainties in those databases, as well as an uncertainty in the instrument functions, on retrieved temperatures. For this case study, we used a pixel number range from 295 to 630, which corresponds to the P-branch of the O_2 *A*-band, for the retrievals. We also arbitrarily selected three scenes per month (November 1996 through June 1997) at each occultation mode (i.e., 24 scenes for each mode) for these simulation studies.

3.1. Molecular oxygen line parameters

Originally, we used HT96 as the O_2 *A*-band line parameters. After the HT96 publication, several experimental studies[3-5] have shown that the line intensities for the O_2 *A*-band are in very good agreement with those of HT96. The air-broadened halfwidth[3] also agrees well with a previous study by Ritter and Wilkerson.[22] However, there was discrepancies in the temperature dependence for the broadening coefficient (hereafter referred to as n_{ab}) and line positions.[3] The value of n_{ab} calculated by Brown and Plymate[3] was 0.63-0.74, depending on quantum numbers, whereas that in HT96 was 0.71 independent of quantum numbers. In this simulation study, we used data from Brown and Plymate for the line intensity and the air-broadened halfwidth. We conducted a sensitivity test on the differences in n_{ab} on retrieved temperature and pressure profiles. The results are shown in Figures 6a and 6b. Below 40 km altitude, the associated temperature error was about 2 K, while the pressure error was about 1%. In these figures, significant oscillations in retrieved profiles are evident both for temperature and pressure profiles between 40 and 55 km altitudes. This is a problem with this retrieval scheme (however, as mentioned in section 3.3, the oscillations can be partly suppressed if higher resolution data are used for the solar spectrum). Although we have been using data from HT96 in the present version of the retrieval algorithm (the Version 5.1), we will replace it with the Brown and Plymate database in the next algorithm version.

3.2. Ozone absorption cross-sections

For an absorption cross-section database of ozone in the Wulf-band region (wavelengths between 700 and 1048 nm), we used data from Brion et al.[16] and the Version 3.5 MODTRAN. Both data were obtained in room temperatures. For the data set of MODTRAN, the cross-section data were taken from Burkholder and Talukdar[23] and references therein. Differences in temperature and pressure retrieved with these two data sets were within 2 K and 1% below 40 km altitude, respectively. Above this altitude, significant oscillations both in temperature and pressure were apparent. In the present algorithm version, we have been using data from Brion et al.,[16] because results of fitting for the baseline component using the Brion et al. data are better than those using the MODTRAN data.

At the present time, there is no absorption cross-section data of ozone at stratospheric temperatures in the wavelength range from 760 nm to 780 nm. Although not shown here, spectral comparisons between the observation and the simulation show that there are some systematic discrepancies between the two spectra in some wavelength regions where the absorption of the O_2 *A*-band is weak (i.e., the transmittance is high.). This is another problem for retrieving temperature and pressure profiles accurately The systematic bias in the ILAS temperatures, mentioned above, might be partly solved by using an accurate O_3 absorption cross-section data at lower temperatures in that wavelength region, if it is available in the near future.

3.3. Solar spectra

In the present algorithm version, we used data from the Version 3.5 MODTRAN as a source function of solar rays in the wavelength from 753 to 784 nm. The spectral resolution of the database is 1 cm^{-1}. Recently, we obtained a higher resolution data set from the Version 5.21 LBLRTM. In this data set, a spectral resolution in the aforementioned wavelength region is 0.025 cm^{-1}. Both data sets were originally taken from Kurucz.[24] We examined the impact of differences in these data sets on retrieved temperature and pressure profiles. Temperature and pressure retrieved using the higher resolution database are in good agreement (within 1 K and 3%, respectively) with those retrieved using the lower resolution one. The use of the high resolution database suppresses oscillations in the retrieved values better than the lower resolution one. Therefore, we will use the higher resolution database in the next algorithm version.

3.4. Instrument functions

As described in section 2.2, the estimated error for the wavelength center of the instrument functions is +/- 0.012 nm. In order to examine a systematic uncertainty associated with these instrument functions, we performed sensitivity tests just by shifting +0.012 nm (or -0.012 nm) for all of the pixels. This amount of error causes temperature errors within 3 K below 40 km altitude both in the northern and southern hemispheres. However, this assumption (i.e., the uniform shift of the wavelength center) may be overdone, so the error associated with the instrument function would be smaller. Above 40 km, the temperature error reveals significant oscillations, reaching errors of more than 5 K on average. For pressure retrievals, the error is estimated to be within 2% below 40 km altitude. Above 40 km, it is estimated to be more than 5%.

4. CONCLUDING REMARKS

Absorption spectra of the molecular oxygen (O_2) *A*-band centered at 762 nm were measured from a visible grating spectrometer of the Improved Limb Atmospheric Spectrometer (ILAS) aboard the Advanced Earth Observing Satellite (ADEOS). The spectral resolution of the spectrometer was 0.17 nm. Because instrument functions are sensitive to instrument temperature due to the optical system of the spectrometer and changes in the instrument temperatures during the ILAS observation period from October 1996 through June 1997 were relatively larger than we had expected, a calibration for the wavelength center of the instrument functions was needed. We could calibrate the wavelength center by the aid of the solar spectra observed by ILAS through exoatmosphere and ground-based very high resolution spectral data in which the wavenumber of the solar lines are well assigned. Considering the probable uncertainties in some databases used in the

ILAS retrieval algorithm, as well as uncertainty in the wavelength center of the instrument functions, we evaluated the impact of these uncertainties on retrieved temperature and pressure profiles. As the result, the error associated with the instrument functions was the largest error source in the systematic uncertainties considered here. The other uncertainties had a smaller impact on the retrieved values. The root-sum-square errors of temperature and pressure associated with the systematic uncertainties considered here were estimated to be 4 K and 4%, respectively, below 40 km altitudes. The error associated with the fitting residuals of convergence (i.e., the internal error) was estimated to be 2 K and 4 K for temperature and 1% and 3% for pressure at altitudes of 20 km and 40 km, respectively. A current problem in the retrieval scheme is that there are scientifically-meaningless oscillations both in the retrieved temperature and pressure, especially above 40 km altitude. This can be partly suppressed by using higher spectral resolution solar line data. Another problem is a lack of the O_3 absorption cross-section data at stratospheric temperatures in the wavelength range from 760 nm to 780 nm, at the present time. There is a possibility that these cross-section data partly compensate systematic discrepancies between the observed and simulated transmittances.

Preliminary comparisons with the HALOE temperatures showed that there was a significant cooling bias in the ILAS temperatures in March, May, and June, 1997 in the northern hemisphere. In contrast, comparisons for November/December, 1996 and January/February, 1997 in the southern hemisphere showed within +/- 5 K differences between the two, sometimes reaching +/- 10 K differences. Another problem in the ILAS retrieval is something related to season and/or occultation mode. These biases can not be explained neither by the systematic nor by the internal errors considered here. Further intensive studies are being conducted to provide better products.

ACKNOWLEDGEMENTS

The authors would like to thank NASDA for its help in making the ILAS project successful. Some data analyses were done by H. Ishihara and K. Niiyama of the ILAS Data Handling Facility (DHF) at NIES and Y. Sato, a Japan Science and Technology Corporation (JST) fellow. The Version 19 HALOE Level 2 data were provided through the NASA/Langley Research Center.

Table 1. Specifications of the visible spectrometer of ILAS

Spectral coverage	753 to 784 nm (13280 to 12755 cm^{-1}) Dispersion: 0.03039+/-0.00017 (1 sigma) nm/pixel Spectral linearity: <2.0%
Optics	Aberration corrected concave holographic grating and 6 plane mirrors. Mirrors: fused quartz, 9 mm, Al surface with SiO_2 coating R = 302.579 +/- 0.017 (1 sigma) mm, f = 401 mm F/16 for dispersion, F/8 for non-dispersion direction, i.e. 1/2 projection Angle between the detector normal and the ray: 15.36 deg Weight: 3.4 kg
Grating	1803 gr./mm (457.93 nm, sine wave), Milton Roy Co. Base: fused quartz, 9 mm Surface: Al with Au coating
Detector	1024 pixels MOS photo diode array, Hamamatsu Photonics Pixel size: 0.020 x 2.000 mm Pixel pitch: 0.025 mm Integration time: 25 msec fixed ADC: 12 bits (11 bits + 1 sign bit) Gain: 1, 2, 5 (nominal in space), and 10

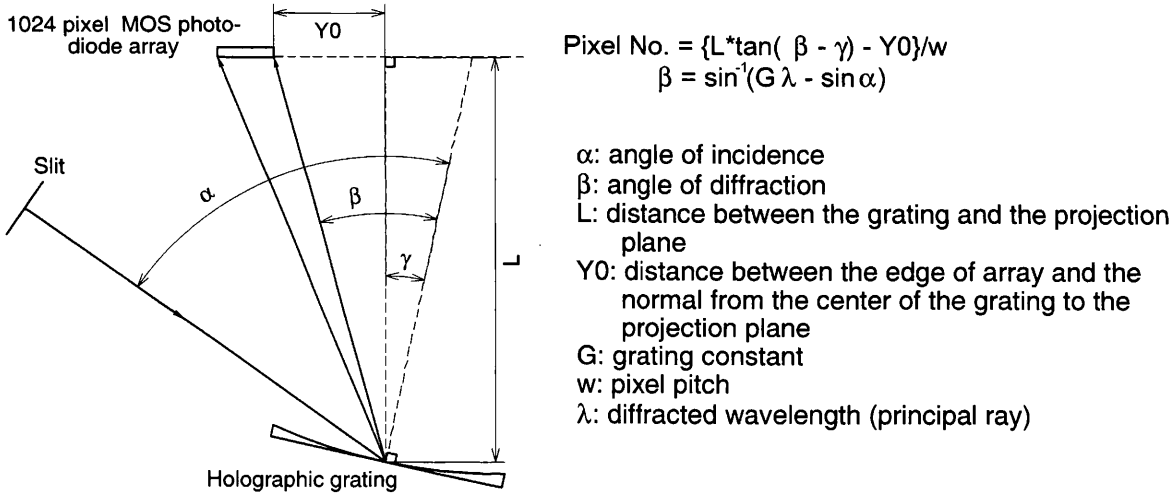

Figure 1. Schematic diagram of the optical system of the visible spectrometer

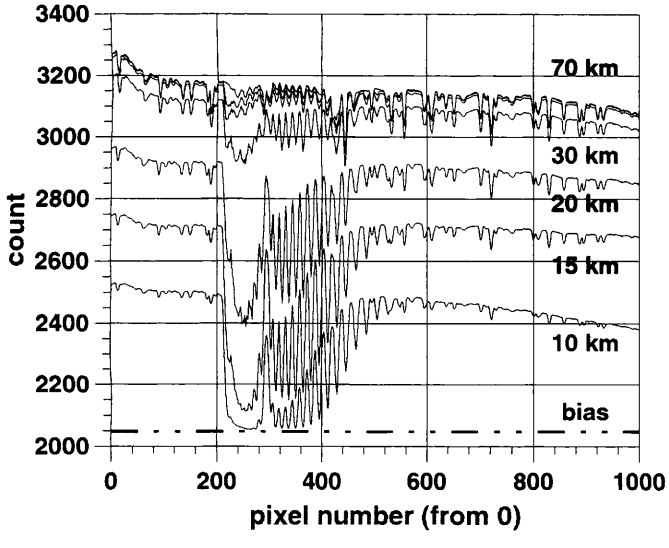

Figure 2. Typical I_a measurements at several tangent heights.

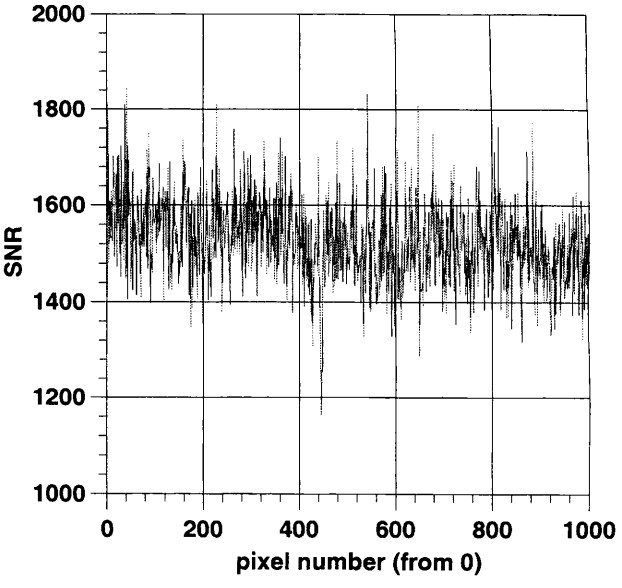

Figure 3. Typical signal-to-noise ratios for the detector.

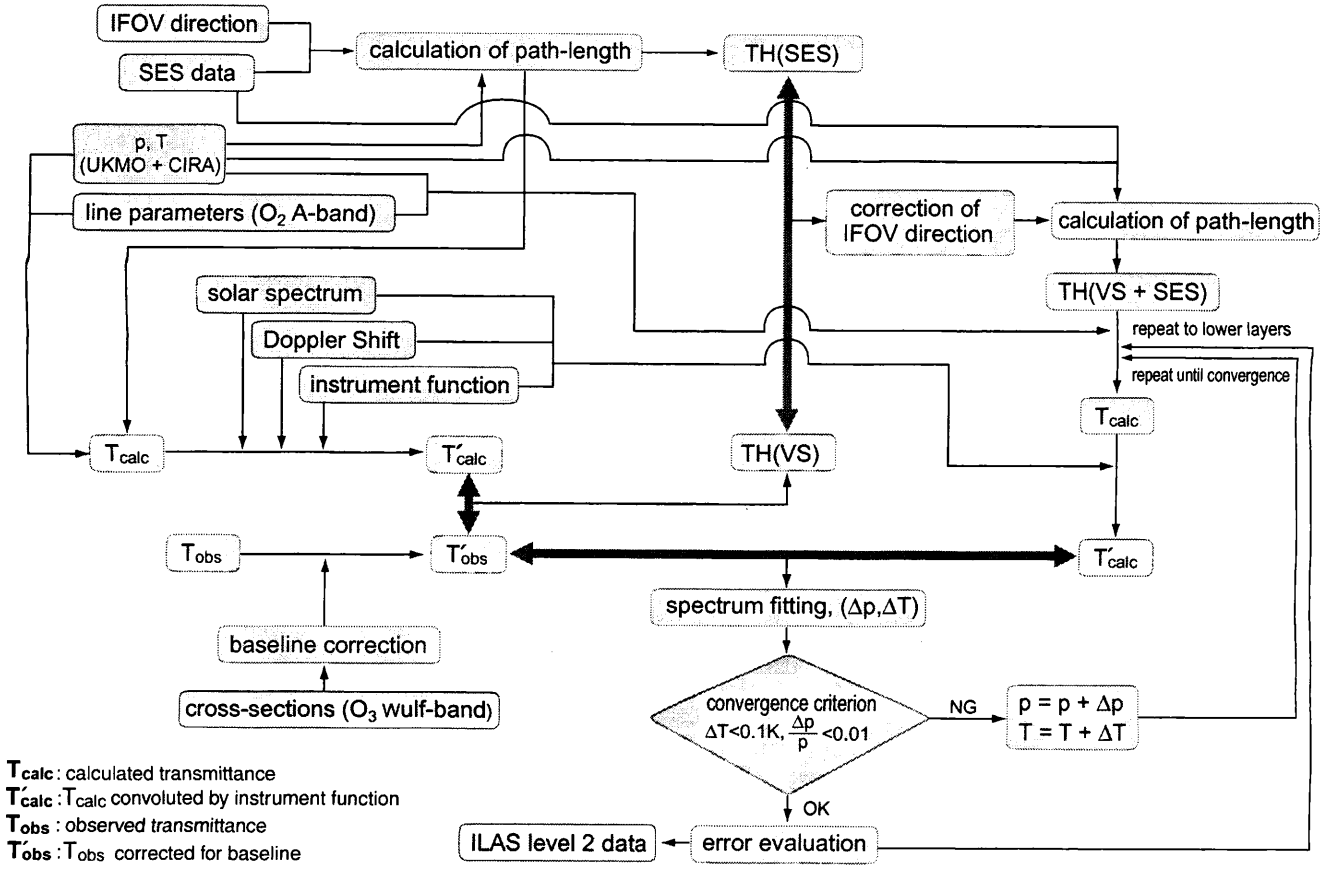

Figure 4. A retrieval flow for profiling temperature and pressure.

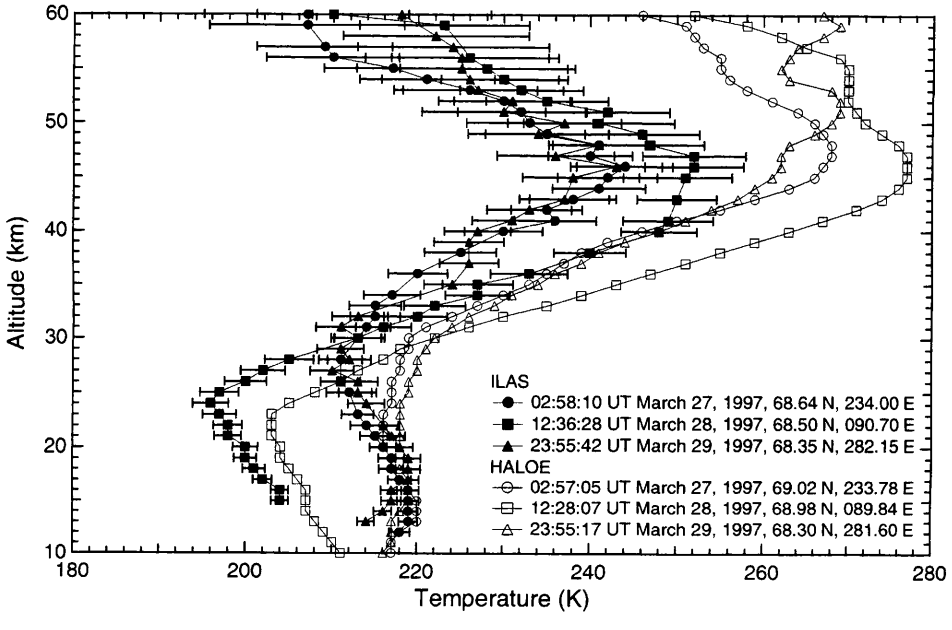

Figure 5. Temperature profiles retrieved by ILAS and HALOE. Times and locations at the tangent height of 20 km are displayed. The bars in the ILAS data show errors associated with residuals of convergence (see section 2.4).

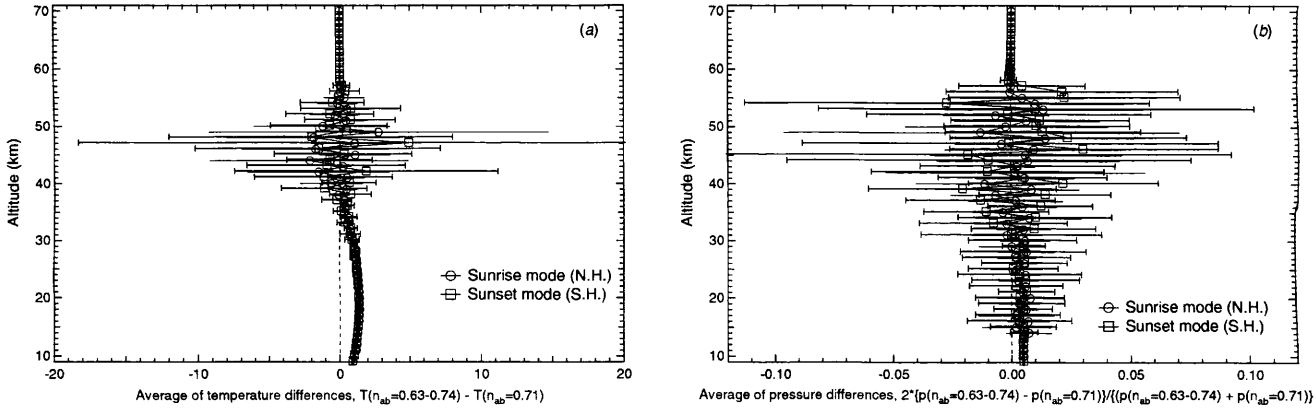

Figure 6. Differences in retrieved temperature (*a*) and pressure (*b*) profiles associated with differences in n_{ab} (see section 3.1).

APPENDIX

The theoretical optical depth at non-uniform wavenumber spacing (like geometrical series), v_k, over the *i*-th line of the O_2 *A*-band for *j*-th layer, is first calculated by a line-by-line algorithm using the Voigt line shape, a convolution of the Lorentz and the Doppler line shape functions.

$$D(v_k) = \sum^{i}\sum^{j} m_j Sl_{ij} \frac{1}{\alpha_{Dij}\sqrt{\pi}} Voigt(x_{ijk}, y_{ij}) \tag{9}$$

where

$$m_j = \int_j \rho_{O2} ds$$

$$Sl_{ij} = s_i \frac{T_0}{T_j} \exp\left\{ A\left(\frac{1}{T_0} - \frac{1}{T_j}\right) E_i \right\} \frac{1 - \exp\left(-A\frac{v_{0i}}{T_j}\right)}{1 - \exp\left(-A\frac{v_{0i}}{T_0}\right)}$$

where

$$\overline{T_j} = \int_j T\rho_{air} ds \Big/ \int_j \rho_{air} ds \,,\ \overline{p_j} = \int_j p\rho_{air} ds \Big/ \int_j \rho_{air} ds \,,\ A = hc/k$$

Here, m_j is the integrated column amount of O_2 molecules along the *j*-th path with an increment (i.e., path element), *ds*, of 1 km, assuming the O_2 mixing ratio of 20.9%. ρ_{O2} and ρ_{air} are the number densities of O_2 molecules and air at each path element, respectively. $\overline{T_i}$ and $\overline{p_i}$ are the so-called "Curtis-Godson temperature and pressure", respectively. T and p is temperature and pressure at each path element. h is the Planck constant, c is the speed of light, and k is the Boltzmann constant. T_0 is 296 K. s_i and E_i is the line intensity and the lower state energy of O_2 molecules in the *A*-band, respectively, at 296 K and at the *i*-th line of HT96. v_{0i} is the line position of the O_2 *A*-band. The Voigt line shape function is expressed as

$$Voigt(x_{ijk}, y_{ij}) = \frac{y_{ij}}{\pi} \int_{-\infty}^{\infty} \frac{\exp(-t^2)}{y_{ij}^{\,2} + (x_{ijk} - t)^2} dt \tag{10}$$

where

$$x_{ijk} = \frac{|\nu_k - \nu_{0i}|}{\alpha_{Dij}}, \quad y_{ij} = \frac{\alpha_{Lij}}{\alpha_{Dij}}$$

$$\alpha_{Dij} = \frac{\nu_{0i}}{c}\sqrt{\frac{2k\overline{T_j}}{m/a_v}}, \quad \alpha_{Lij} = \alpha_{L0i}\frac{\overline{p_j}}{p_0}\left(\frac{T_0}{\overline{T_j}}\right)^{t_{ni}}$$

Here, α_{Lij} and α_{Dij} are the Lorentzian half-width and the Doppler half-width, respectively, at the i-th line and the j-th layer. m is the molecular weight of O_2 molecules, and a_v is the Avogadro number. α_{L0i} and t_{ni} are the air-broadened half-width and the coefficient of temperature dependence of α_{L0i}, respectively, at the i-th line of the O_2 A-band. To compute the Voigt line shape function, we used the method proposed by Hui et al.[26] The $D(\nu_k)$ derived by the above procedure is converted to transmittance (appearing in Equation (2)) by Equation (11).

$$\tau'_c(\nu_k) = \exp\{-D(\nu_k)\} \tag{11}$$

REFERENCES

1. Y. Sasano *et al.*, "Improved limb atmospheric spectrometer (ILAS) for stratospheric ozone layer measurements by solar occultation technique," *Geophys. Res. Lett.* **26**, pp. 197-200, 1999.
2. Y. Sasano *et al.*, "Validation of ILAS Version 3.10 ozone with ozonesonde measurements," *Geophys. Res. Lett.* **26**, pp. 831-834, 1999.
3. L. R. Brown and C. Plymate, "Experimental line parameters of the oxygen A band at 760 nm," *J. Mol. Spectrosc.* **199**, pp. 166-179, 2000.
4. S. F. Yang *et al.*, "Intensity measurements and collision-broadening coefficients for the oxygen A band measured by intracavity laser absorption spectroscopy," *J. Mol. Spectrosc.* **201**, pp. 188-197, 2000.
5. R. Schermaul and R. C. M. Learner, "Precise line parameters and transition probability of the atmospheric A band of molecular oxygen $^{16}O_2$," *J. Quant. Spectrosc. Radiat. Transfer* **61**, pp. 781-794, 1999.
6. L. Wallace and D. M. Hunten, "Dayglow of the oxygen A band," *J. Geophys. Res.* **73**, pp. 4813-4834, 1968.
7. J. W. Heller *et al.*, "Mesospheric temperature inferred from daytime observation of the O_2 atmospheric (0,0) band system," *J. Geophys. Res.* **96**, pp. 19,499-19,505, 1991.
8. A. Matsuzaki, Y. Nakamura and T. Itoh, "Rocket observation of the rotational profile of the A-band absorption spectrum of atmospheric oxygen molecule," *Ann. Geophysicae* **2**, pp. 475-480, 1984.
9. M. C. Pitts and L. W. Thomason, "Remote sensing of temperature and pressure by the Stratospheric Aerosol and Gas Experiment III," *The EUROPTO Conference on Satellite Remote Sensing of Clouds and the Atmosphere IV*, J. E. Russell ed. pp. 206-215, SPIE, Florence, Italy, 1999.
10. M. C. Pitts, "Retrieval of temperature and pressure profiles for the Stratospheric Aerosol and Gas Experiment III," Ph.D. thesis, pp. 162, The College of William and Mary, 1999.
11. T. Nakajima, Y. Sasano and M. Suzuki, "Visible remote sensing algorithms for the improved limb atmospheric spectrometer aboard ADEOS satellite," *IRS '92: Current Problems in Atmospheric Radiation*, S. Keevallik and O. Kärner eds., pp. 383-385, A. Deepak Publishing, Tallinn, Estonia, 1993.
12. L. Wallace, K. Hinkle and W. Livingston, "An atlas of the solar photospheric spectrum in the region from 8900 to 13600 cm^{-1} (7350 to 11230 Å) with decomposition into solar and atmospheric components and identifications of the main solar features," National Solar Observatory, National Optical Astronomy Observatories, N.S.O. Technical Report No. 93-001, Tucson, AZ, 1993.
13. H. Nakajima *et al.*, "Characteristics and performance of the Improved Limb Atmospheric Spectrometer (ILAS) in orbit," *J. Geophys. Res.* **in preparation**.
14. O. R. Wulf, "The band spectrum of ozone in the visible and photographic infra-red," *Proc. Natl. Acad. Sci.* **16**, pp. 507-511, 1930.
15. S. Hayashida *et al.*, "Arctic polar stratospheric clouds observed with the Improved Limb Atmospheric Spectrometer during the winter of 1996/1997," *J. Geophys. Res.* **105**, pp. 24,715-24,730, 2000.
16. J. Brion *et al.*, "Absorption spectra measurements for the ozone molecule in the 350-830 nm region," *J. Atmos. Chem.* **30**, pp. 291-299, 1998.

17. A. Berk, L. S. Bernstein and D. C. Robertson, "MODTRAN: A Moderate Resolution Model for LOWTRAN 7," Air Force Geophys. Lab., GL-TR-89-0122, Hanscom AFB, MA, 1989.
18. R. Swinbank and A. O'Neill, "A stratosphere-troposphere data assimilation system," *Mon. Weather Rev.* **122**, pp. 686-702, 1994.
19. E. L. Fleming *et al.*, "Zonal mean temperature, pressure, zonal wind, and geopotential height as functions of latitude, COSPAR International Reference Atmosphere: 1986, Part II: Middle Atmosphere Models," *Adv. Space Res.* **10**, pp. 11-59, 1990.
20. R. R. Gamache, A. Goldman and L. S. Rothman, "Improved spectral parameters for the three most abundant isotopomers of the oxygen molecule," *J. Quant. Spectrosc. Radiat. Transfer* **59**, pp. 495-509, 1998.
21. H. Nakajima *et al.*, "Tangent height registration for the solar occultation satellite sensor ILAS: a new technique for Version 5.00 products and its validation," *J. Geophys. Res.* **in preparation**.
22. K. J. Ritter and T. D. Wilkerson, "High-resolution spectroscopy of the oxygen *A* band," *J. Mol. Spectrosc.* **121**, pp. 1-19, 1987.
23. J. B. Burkholder and R. K. Talukdar, "Temperature dependence of the ozone absorption spectrum over wavelength range 410 to 760 nm," *Geophys. Res. Lett.* **21**, pp. 581-584, 1994.
24. R. L. Kurucz, "Synthetic infrared spectra," in *Infrared solar physics*, D. M. Rabin and J. T. Jefferies eds., pp. Kluwer, Tucson, AZ, 1994.
25. M. E. Hervig *et al.*, "Validation of temperature measurements from the Halogen Occultation Experiment," *J. Geophys. Res.* **101**, pp. 10,277-10,285, 1996.
26. A. K. Hui, B. H. Armstrong and A. A. Wary, "Rapid computation of the Voigt and complex error functions," *J. Quant. Spectrosc. Radiat. Transfer* **19**, pp. 509-516, 1978.